P H Y S I C A L   R E V I E W   L E T T E R S

Strong-Field Dissociative Double Ionization of Acetylene

Xiaochun Gong, Qiying Song, Qinying Ji, Haifeng Pan, Jingxin Ding, Jian Wu,[*] and Heping Zeng

State Key Laboratory of Precision Spectroscopy, East China Normal University, Shanghai 200062, China

We investigate dissociative double ionization of acetylene, one of the smallest organic molecules yet with a rich electronic structure, in strong laser fields by measuring two fragment ions and two electrons in coincidence. The two-body fragmentation channels are dominated by the removal of electrons from the lower-lying molecular orbitals rather than from the highest occupied one. The electron localization-assisted enhanced ionization mechanism plays a central role for the strong-field deprotonation ionization of acetylene by releasing the second electron from the up-field potential well of the hydrogen site at the internuclear distance near twice the equilibrium value of the C-H bond.

Correlated ultrafast electron-nuclear motion [1–4] is one of the most fundamental and fascinating phenomena of a molecule irradiated by photons. On the one hand, instantaneous removal of electrons from a molecule alters the potential between the nuclei and initiates the nuclear motion, resulting in molecular structure changes, bond breakage, and chemical reaction. On the other hand, the nuclear motion rearranges the distribution of the remaining electrons and hence remodels their response to the light. It is therefore a key ingredient to understand and control the complex photoinduced dynamics of molecules.

As one of the most prominent manifestations of electron-nuclear dynamics in strong laser fields, a molecule experiences a significantly enhanced ionization rate if the molecular axis is parallel to the field vector [5–12]. This electron localization-assisted enhanced ionization mechanism is generally found in strong-field multielectron ionization of diatomic [7–12] and triatomic molecules [13,14]. The vast majority of molecules, however, are polyatomic (e.g., hydrocarbon) molecules. Interestingly, it was recently numerically demonstrated [15,16] that the enhanced ionization mechanism plays an important role in deprotonation ionization of the smallest linear hydrocarbon molecule of acetylene (C_2H_2). The model correctly predicts the observed all-at-once ejection of high-energy protons in strong-field multielectron ionization of small hydrocarbon molecules [17,18]. However, the cornerstone of the electron localization-assisted enhanced ionization scenario in the deprotonation ionization of the hydrocarbon molecule has not yet been verified experimentally, i.e., that the localized electron is indeed released from the up-field potential well and the critical dependence on the internuclear distance [8,19,20].

In this Letter, we study the interplay of the electron-nuclear dynamics of small hydrocarbon molecules in strong laser fields using dissociative double ionization of acetylene as a prototype. By measuring two fragment ions and two electrons ejected from a doubly ionized acetylene molecule in coincidence, we show that the two-body

fragmentation channels are dominated by the removal of electrons from the lower-lying molecular orbitals rather than from the highest occupied one. Remarkably, our results verify the important role of the electron localization-assisted enhanced ionization in the strong-field deprotonation ionization of acetylene.

The measurements were performed in a standard reaction microscope of cold target recoil ion momentum spectroscopy [21,22] as schematically illustrated in Fig. 1. We focused elliptically polarized femtosecond laser pulses (25 fs, 790 nm, 10 kHz) produced from a multipass amplifier Ti:sapphire laser system onto a supersonic gas jet by a concave reflection mirror ($f = 7.5$ cm) inside the apparatus. The peak intensity and ellipticity of the laser pulse were measured to be $I_0 = 2 \times 10^{14}$ W/cm^2 and $\varepsilon = 0.56$. The major and minor polarization axes of the laser pulse are along the y and z axes, respectively. The laser field (yellow helix) rotated clockwise from $+z$ to $+y$ in the y-z (polarization) plane and propagated along the $-x$ axis after the focusing mirror. The molecular jet propagating along the y axis was produced by coexpanding a mixture of 5% C_2H_2 and 95% He through a 30 μm nozzle with a driving pressure of 2 bar. We estimated the jet density of $\sim 1.5 \times 10^7$ cm^{-3} for C_2H_2 in the interaction region. By measuring the momentum distribution of $C_2H_2^+$ along the jet direction $\Delta p_y = 4.1$ a.u. we estimated the translational temperature of our jet $T_{\text{trans}} = \Delta p_y^2/[4\ln(4)k_Bm] \sim 20$ K [23]. Here, k_B and m are the Boltzmann constant and mass of the singly ionized acetylene, respectively. By suppressing the electron recollision processes [24,25], our elliptically polarized laser pulse sequentially removed electrons from a molecule, allowing us to study each individual ionization step. The ions and electrons ejected from an exploding molecule were detected in coincidence by two time- and position-sensitive microchannel plate detectors [26] at the opposite ends of the spectrometer.

In a close-to-circularly polarized laser pulse, the direction and intensity of the laser field at the instant of ionization are
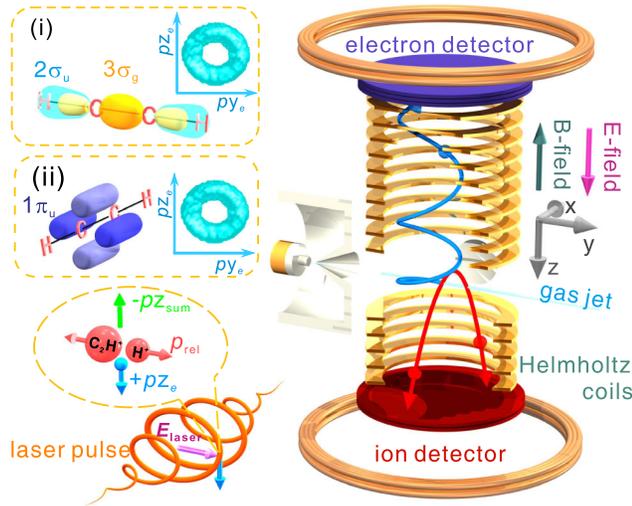
FIG. 1 (color online). Schematic diagram of the experimental apparatus. The insets schematically illustrate that (i) both the molecular axis of the acetylene and the freed electrons (blue donut) lie in the polarization plane for the dominance of the σ orbitals, whereas (ii) the acetylene is oriented perpendicular to the polarization plane for the dominance of the π orbital.

encoded in the measured momentum of the ejected electron in the polarization plane [27,28]. We therefore restrict our data analysis and discussion to such electrons ejected in the polarization plane ($|\theta_{xe} - 90°| < 30°$). Here, θ_{xe} and θ_{xmol} are the polar angles of the ejected electrons and fragment ions with respect to the x axis, respectively. As illustrated in the insets of Fig. 1, the participation of the (i) σ or (ii) π orbitals is correlated to the fragment ions ejected (i) in ($|\theta_{xmol} - 90°| < 30°$) or (ii) perpendicular ($|\theta_{xmol}| < 30°$ or $|\theta_{xmol} - 180°| < 30°$) to the polarization plane, respectively. We assume that the excitation of the bending mode and the geometric rotation of the molecule are insignificant during the ultrafast ionization and fragmentation in ultrashort laser pulses [29]. This is supported by the observed correlated narrow angular distributions of the fragment ions in our experiment (see Supplemental Material [30]). Since both the electrons and fragment ions lie in the laser polarization plane for the ionization of the σ orbital, the molecular-frame photoelectron angular distribution (MFPAD) (ϕ_e^{mol}) [33] and momentum distribution ($p_{e//}^{mol}$ vs $p_{e\perp}^{mol}$) are reconstructed, in which the ejection direction of the ionic fragment H^+ (CH^+ or C^+ for various channels) is rotated to the direction of $\phi_e^{mol} = 0°$. The $p_{e//}^{mol}$ and $p_{e\perp}^{mol}$ are the electron momenta parallel and perpendicular to the molecular axis, respectively.

As schematically shown in the insets of Fig. 1, for acetylene, the electron density of the highest occupied molecular orbital (HOMO) ($1\pi_u$) distributes perpendicularly to the molecular axis, whereas that of the HOMO-1 ($3\sigma_g$) orbital distributes in both the C-C and C-H bonds and that of the HOMO-2 ($2\sigma_u$) orbital in the C-H bond along the molecular axis. For the equilibrium geometry of acetylene ($R_{CC} \sim 2.2$ and $R_{CH} \sim 2$ a.u.), the binding energies of the HOMO, HOMO-1, and HOMO-2 orbitals are 11.4, 16.6,

and 18.8 eV [16], respectively. The double ionization is dominated by the removal of two electrons from the weakly bound HOMO which mostly populates the ground state of the dication. It results in the here-observed ratios of 87% for the nondissociative $C_2H_2^{2+}$ and 13% for the total yield of the two-body fragmentation channels. As we will show in the following, the fragmentation channels are governed by the removal of electrons from the HOMO-1 or HOMO-2; nevertheless, the removal of electrons from the HOMO also participates. In our experiment, the double ionization induced deprotonation [denoted (H^+, C_2H^+)], symmetric [denoted (CH^+, CH^+)], and isomerization [denoted (C^+, CH_2^+)] dissociation channels are all observed, whose branching ratios to the total two-body fragmentation yield are 58%, 19%, and 23%, respectively.

We start with the (H^+, C_2H^+) channel accompanied by the C-H bond breakage. Figures 2(a) and 2(b) show the momentum distributions of the emitted two electrons correlated to the fragment ions ejected (i) in and (ii) perpendicular to the polarization plane, respectively, corresponding to the dominance of the (i) σ and (ii) π symmetric orbitals. The relative contribution of the removal of two π symmetric HOMO electrons [case (ii) as shown in Fig. 2(b)] as compared to that dominated by the σ orbitals [case (i) as shown in Fig. 2(a)] is indicated by their yield ratio ($\sim 4.8 \pm 0.1$%) as presented in Fig. 2(c). The small contribution of the case (ii) in producing the (H^+, C_2H^+) channel is consistent with the fact that the removal of two HOMO electrons mainly leads to the nondissociative $C_2H_2^{2+}$. In the following, we will focus on the case (i), in which the dominant σ orbital can be the HOMO-1 or HOMO-2 since they together make the C-H bond [see inset (i) of Fig. 1] [16]. Although the HOMO electron is preferred to be freed when the acetylene is oriented orthogonally to the field direction, as shown in Ref. [16], the HOMO still shows a much higher ionization probability as compared to the HOMO-1 and HOMO-2 at the equilibrium internuclear distance when the acetylene is oriented parallel to the field direction. This is due to the low binding energy of the HOMO. For case (i), the first electron is most likely to be removed from the HOMO at the equilibrium internuclear distance, and then the second electron from the HOMO-1 or HOMO-2 at a stretched internuclear distance. The removal of one electron from the HOMO is symmetric with respect to the laser field direction and molecular orientation during the first ionization stage. The asymmetric MFPAD shown in Fig. 2(d) must originate from the second ionization step, which is favored when the laser field points to the hydrogen site. It is opposite to the prediction of the molecular Ammosov-Delone-Krainov theory [34,35] (the electron density shifts to the hydrogen site in the C-H bond), but agrees with the scenario of electron localization-assisted enhanced ionization [8,19,20]. As illustrated in Fig. 1, the electron (blue ball) released by laser field along $\pm y$ ends with momentum along $\pm z$ (blue arrow) after the clockwise rotating laser
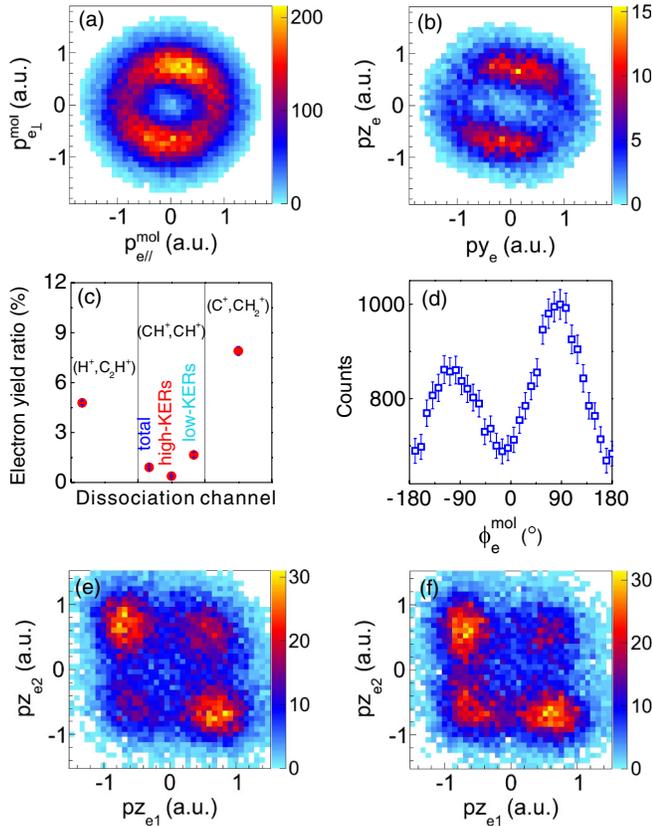
FIG. 2 (color online).   (a),(b) The measured momentum distributions of two electrons on top of each other for the (H^+, C_2H^+) channel when the correlated fragment ions emit (a) in and (b) perpendicular to the polarization plane, respectively. (c) The yield ratios of the electron correlated to fragment ions emitting perpendicular to the polarization plane to that correlated to fragment ions emitting in the polarization plane for the here-observed two-body dissociation channels. (d) The MFPAD of the (H^+, C_2H^+) channel. (e),(f) The pz_{e1} vs pz_{e2} for the (H^+, C_2H^+) channel when the H^+ departs to (e) $+y$ and (f) $-y$, respectively.

pulse. The divergence of the maxima in MFPAD from $\pm 90°$ [see Fig. 2(d)] indicates the attractive Coulomb potential effect [36] of the ionic core on the escaping electrons.

In addition to the MFPAD, as shown in Figs. 2(e) and 2(f), the laser field direction dependence of the second ionization stage can be directly observed in the laboratory frame by inspecting the momenta of the two freed electrons along z, i.e., pz_{e1} vs pz_{e2}, when the ejection direction of the H^+ is gated to $+y$ or $-y$. The distributions in the second and fourth quadrants of Figs. 2(e) and 2(f) stand for the removal of two electrons by laser fields pointing to opposite directions along the y axis. The first and third quadrants are registered when both electrons are released by laser fields pointing to $+y$ and $-y$, respectively. Interestingly, for H^+ departing to $+y$ as shown in Fig. 2(e) [or $-y$ as shown in Fig. 2(f)], there are more (or less) electrons distributed in the first quadrant than the third quadrant with a count ratio of 1.4 ± 0.06 (or 0.66 ± 0.03). It indicates that the second electron is favored to be freed by laser field pointing to

hydrogen for the (H^+, C_2H^+) channel, which agrees with the observed asymmetric MFPAD as shown in Fig. 2(d).

Because of momentum conservation of the ejected electrons and ions, the laser field direction along the y axis at the ionization moment is encoded in the sum momentum of correlated fragment ions along the z axis, i.e., $pz_{sum} = -pz_{e1} - pz_{e2}$. By merely detecting two fragment ions, the statistical significance of the data is increased and the possible ambiguity due to the dead time in two electron detection is avoided. As displayed in Fig. 3(a), the enhancement in rate at $+pz_{sum}$ (or $-pz_{sum}$) when H^+ departs to $-y$ (or $+y$) corresponds to the favored electron distribution in the first (or third) quadrant of Fig. 2(e) [or Fig. 2(f)]. To get a more detailed insight in the dependence of the second electron emission on the laser field direction, we numerically fitted the momentum distribution of pz_{sum} with the convolution of the two sequentially released electrons [20]. Figure 3(b) shows a clear dependence of the asymmetry $\beta = (A_{e2,H+} - A_{e2,C2H+})/(A_{e2,H+} + A_{e2,C2H+})$ (blue solid squares) on the kinetic energy release (KER) of fragment ions. Here, $A_{e2,H+}$ and $A_{e2,C2H+}$ are the releasing probabilities of the second electron by the laser field pointing to H^+ or C_2H^+, respectively. It indicates the dependence of the asymmetry parameter β on the C-H distance at the second ionization stage (higher KER corresponds to a shorter C-H distance). As shown in Fig. 3(b), the value of β increases first and then decreases with a maximum around KER ~ 4.2 eV. To estimate the internuclear distance with the KER, i.e., KER$\sim 1/[R_{CH} + 0.5(R_{CC} + R_{CH})]$, we assume a Coulomb explosion between the point charges at the proton and the center of the H-C-C bonds. This approximation is justified at the large distance of R_{CH} where the potential energy curve of the $^3\Pi_u$ state [37] accessed by removing one HOMO electron and one HOMO-2 electron for the (H^+, C_2H^+) channel is very close to the Coulombic potential. By assuming the equilibrium internuclear distance of $R_{CC} \sim 2.2$ a.u., we estimate $R_{CH} \sim 3.6$ a.u. for the KER of 4.2 eV. It is comparable to the values obtained in recent numerical calculations [15,16]. The large error bars in Fig. 3(b) at high KERs are due to the decreased yield of the (H^+, C_2H^+) channel in this KER range [see the KER spectrum in the inset of Fig. 3(a)]. Without the mechanism of electron localization, the ionization probabilities of both the HOMO-1 and HOMO-2 orbitals decrease at short R_{CH} owing to the increased binding energies [16], where a high laser intensity is responsible for the ionization. As shown in Fig. 3(b), the required high laser intensity at the ionization increases the final momentum (red open squares) of the electron gained from the rotating laser field.

By observing the unique properties of the laser field direction and internuclear distance dependences of the removal of the second electron, our results experimentally verify the central role of electron localization-assisted enhanced ionization in strong-field deprotonation ionization of acetylene.
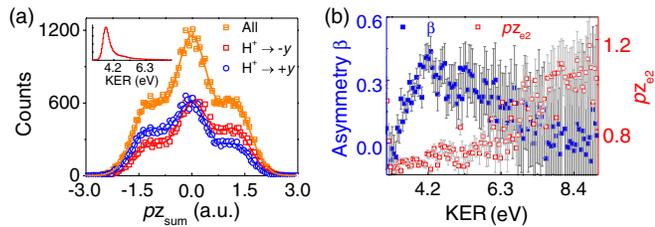
FIG. 3 (color online). (a) The ion sum-momentum distributions of the (H^+, C_2H^+) channel. The inset shows the KER distribution. (b) The fitted momentum of the second electron pz_{e2} and the asymmetry parameter β as a function of KER for the (H^+, C_2H^+) channel.

We now turn to the (CH^+, CH^+) channel accompanied by the C-C bond breakage. As shown in Fig. 4(a), there are two distinct KER distributions labeled as high and low KERs separated around 5.5 eV. It indicates the removal of electrons at different internuclear distances of R_{CC} or dissociation from different states of the dication with different excess energies available for the fragment ions. The separation between the two KER peaks does not depend on the photon energy of the employed laser pulse (see Supplemental Material [30]). Interestingly, as shown in the inset of Fig. 4(a), the relative yield of the high KERs increases as compared to the low KERs when the laser intensity increases. It is consistent with the observed relative contribution of the π orbital as compared to the dominant σ orbital for the high and low KERs. As presented in Fig. 2(c), the negligible contribution ($\sim 0.38 \pm 0.06\%$) of the π orbital at high KERs indicates that the high KER region is governed by the electron removal from the tightly bound σ orbital, whose ionization possibility increases as the increasing laser intensity. On the other hand, as shown in Fig. 2(c), although there is a small contribution ($\sim 1.7 \pm 0.1\%$) of the removal of two electrons from the π symmetric HOMO for the (CH^+, CH^+) channel at low KERs, the lower-lying σ orbital nevertheless dominates the production of low KER ions. As compared to the nonsequential double ionization by low-intensity few-cycle laser pulse [38], the (CH^+, CH^+) channel is preferred to emit ions along the field direction in our 25 fs laser pulse at an intensity higher than 1×10^{14} W/cm^2 (see Supplemental Material [30]).

Interestingly, as an indicator of intramolecular proton migration from one C atom to the other, we observed a considerable yield of the (C^+, CH_2^+) channel. For its significance in understanding the chemical and biological processes [39], the photoisomerization of acetylene has been the subject of numerous experimental [37,40–49] and theoretical [50–53] studies. As compared to the excitation by extreme ultraviolet pulses [40], where the isomerization mainly occurs on the cation state (indicated by the yielded high KERs peaked at 5.8 eV), our intense near-infrared laser pulse initiates the isomerization on the $C_2H_2^{2+}$ dication state [42,45], resulting in KERs mainly below 5.0 eV [see Fig. 4(b)]. It, for instance, populates the excited

$1^3\Pi$ state of the $C_2H_2^{2+}$ dication where the isomerization can proceed rapidly [40,42]. Although it differs from the isomerization excited by synchrotron radiation [46–49], we observed an $\sim 8 \pm 0.3\%$ contribution of the removal of two HOMO electrons for the (C^+, CH_2^+) channel as compared to that governed by the σ orbital [see Fig. 2(c)] in our near-infrared laser pulse. As compared to the (H^+, C_2H^+) [Fig. 2(d)] and (CH^+, CH^+) channels [Fig. 4(c)], the more isotropic MFPAD of the (C^+, CH_2^+) channel [Fig. 4(d)] could indicate a slight rotation (20°) or vibrational excitation of the molecule during the intramolecular proton migration [46] before the C-C bond breakage. It is consistent with the observed relatively broader angular distribution of the fragment ions for the (C^+, CH_2^+) channel as compared to the (H^+, C_2H^+) and (CH^+, CH^+) channels (see Supplemental Material [30]).

In summary, by measuring two fragment ions and two electrons in coincidence, we have experimentally investigated the strong-field dissociative double ionization of acetylene. Our results on the one hand demonstrate that the two-body fragmentation channels are governed by the removal of electrons from the lower-lying molecular orbitals; on the other hand, they experimentally verify the central role of the electron localization-assisted enhanced ionization mechanism in the strong-field deprotonation ionization of acetylene. Our present work will shed some light on the understanding and controlling of the rich electron-nuclear dynamics of complex polyatomic, in particular hydrocarbon, molecules [15–18,41–44,53–55] in strong laser fields.
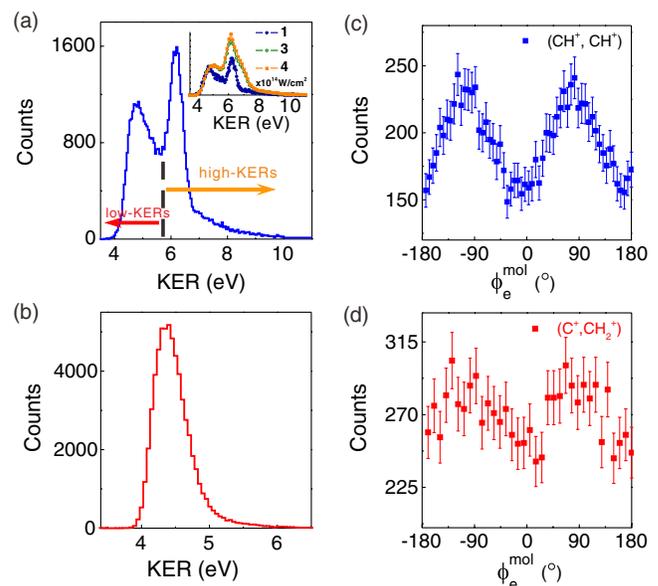
FIG. 4 (color online). (a) The KER distribution of the (CH^+, CH^+) channel at the laser intensity of 2×10^{14} W/cm^2. The inset shows the KER distributions at various laser intensities of 1×10^{14}, 3×10^{14}, and 4×10^{14} W/cm^2, respectively. (b) The KER distribution of the (C^+, CH_2^+) channel. (c),(d) The MFPADs of (c) the (CH^+, CH^+) channel, and (d) the (C^+, CH_2^+) channel, respectively.

*jwu@phy.ecnu.edu.cn

[1] E. Gagnon, P. Ranitovic, X. M. Tong, C. L. Cocke, M. M. Murnane, H. C. Kapteyn, and A. S. Sandhu, Science **317**, 1374 (2007).

[2] A. N. Markevitch, D. A. Romanov, S. M. Smith, and R. J. Levis, Phys. Rev. A **75**, 053402 (2007).

[3] O. Smirnova, Y. Mairesse, S. Patchkovskii, N. Dudovich, D. Villeneuve, P. Corkum, and M. Y. Lvanov, Nature (London) **460**, 972 (2009).

[4] X. Zhou, P. Ranitovic, C. W. Hogle, J. H. D. Eland, H. C. Kapteyn, and M. M. Murnane, Nat. Phys. **8**, 232 (2012).

[5] L. J. Frasinski, K. Codling, P. Hatherly, J. Barr, I. N. Ross, and W. T. Toner, Phys. Rev. Lett. **58**, 2424 (1987).

[6] E. Constant, H. Stapelfeldt, and P. B. Corkum, Phys. Rev. Lett. **76**, 4140 (1996).

[7] W. T. Hill, III, J. Zhu, D. L. Hatten, Y. Cui, J. Goldhar, and S. Yang, Phys. Rev. Lett. **69**, 2646 (1992).

[8] T. Zuo and A. D. Bandrauk, Phys. Rev. A **52**, R2511 (1995).

[9] K. Codling, L. J. Frasinski, and P. A. Hatherly, J. Phys. B **22**, L321 (1989).

[10] M. Schmidt, D. Normand, and C. Cornaggia, Phys. Rev. A **50**, 5037 (1994).

[11] D. M. Villeneuve, M. Y. Ivanov, and P. B. Corkum, Phys. Rev. A **54**, 736 (1996).

[12] G. L. Kamta and A. D. Bandrauk, Phys. Rev. Lett. **94**, 203003 (2005).

[13] I. Bocharova et al., Phys. Rev. Lett. **107**, 063201 (2011).

[14] J. Wu, X. Gong, M. Kunitski, F. K. Amankona-Diawuo, L. Ph. H. Schmidt, T. Jahnke, A. Czasch, T. Seideman, and R. Dörner, Phys. Rev. Lett. **111**, 083003 (2013).

[15] E. Lötstedt, T. Kato, and K. Yamanouchi, Phys. Rev. A **85**, 041402(R) (2012).

[16] E. Lötstedt, T. Kato, and K. Yamanouchi, J. Chem. Phys. **138**, 104304 (2013).

[17] S. Roither et al., Phys. Rev. Lett. **106**, 163001 (2011).

[18] S. Bubin, M. Atkinson, K. Varga, X. Xie, S. Roither, D. Kartashov, A. Baltuška, and M. Kitzler, Phys. Rev. A **86**, 043407 (2012).

[19] T. Seideman, M. Y. Ivanov, and P. B. Corkum, Phys. Rev. Lett. **75**, 2819 (1995).

[20] J. Wu, M. Meckel, L. Ph. H. Schmidt, M. Kunitski, S. Voss, H. Sann, H. Kim, T. Jahnke, A. Czasch, and R. Dörner, Nat. Commun. **3**, 1113 (2012).

[21] R. Dörner, V. Mergel, O. Jagutzki, L. Spielberger, J. Ullrich, R. Moshammer, and H. Schmidt-Böcking, Phys. Rep. **330**, 95 (2000).

[22] J. Ulrich, R. Moshammer, A. Dorn, R. Dörner, L. Ph. H. Schmidt, and H. Schmidt-Böcking, Rep. Prog. Phys. **66**, 1463 (2003).

[23] J. Wu, A. Vredenborg, B. Ulrich, L. Ph. H. Schmidt, M. Meckel, S. Voss, H. Sann, H. Kim, T. Jahnke, and R. Dörner, Phys. Rev. A **83**, 061403(R) (2011).

[24] A. N. Pfeiffer, C. Cirelli, M. Smolarski, R. Dörner, and U. Keller, Nat. Phys. **7**, 428 (2011).

[25] Y. Zhou, C. Huang, Q. Liao, and P. Lu, Phys. Rev. Lett. **109**, 053004 (2012).

[26] O. Jagutzki et al., IEEE Trans. Nucl. Sci. **49**, 2477 (2002).

[27] P. Eckle, M. Smolarski, P. Schlup, J. Biegert, A. Staudte, M. Schöffler, H. G. Muller, R. Dörner, and U. Keller, Nat. Phys. **4**, 565 (2008).

[28] J. Wu et al., Nat. Commun. **4**, 2177 (2013).

[29] A. Staudte et al., Phys. Rev. Lett. **102**, 033004 (2009).

[30] See Supplemental Material at http://link.aps.org/supplemental/10.1103/PhysRevLett.112.243001 for details on the field-intensity-dependent enhanced ionization, angular and kinetic-energy-release distributions of the fragmentation channels, which includes Refs. [31] and [32].

[31] S. Chelkowski and A. D. Bandrauk, J. Phys. B **28**, L723 (1995).

[32] A. S. Alnaser, C. M. Maharjan, X. M. Tong, B. Ulrich, P. Ranitovic, B. Shan, Z. Chang, C. D. Lin, C. L. Cocke, and I. V. Litvinyuk, Phys. Rev. A **71**. 031403(R) (2005).

[33] K. L. Reid, Mol. Phys. **110**, 131 (2012).

[34] X. M. Tong, Z. X. Zhao, and C. D. Lin, Phys. Rev. A **66**, 033402 (2002).

[35] O. I. Tolstikhin, T. Morishita, and L. B. Madsen, Phys. Rev. A **84**, 053423 (2011).

[36] M. Odenweller, N. Takemoto, A. Vredenborg, K. Cole, K. Pahl, J. Titze, L. Ph. H. Schmidt, T. Jahnke, R. Dörner, and A. Becker, Phys. Rev. Lett. **107**, 143004 (2011).

[37] R. Thissen, J. Oelwiche, J. M. Robbe, D. Duflot, J. P. Flament, and J. H. D. Eland, J. Chem. Phys. **99**, 6590 (1993).

[38] C. D. Lin, X. M. Tong, and Z. X. Zhao, J. Mod. Opt. **53**, 21 (2006).

[39] D. Polli et al., Nature (London) **467**, 440 (2010).

[40] Y. H. Jiang et al., Phys. Rev. Lett. **105**, 263002 (2010).

[41] A. S. Alnaser et al., J. Phys. B **39**, S485 (2006).

[42] A. Hishikawa, A. Matsuda, M. Fushitani, and E. J. Takahashi, Phys. Rev. Lett. **99**, 258302 (2007).

[43] H. Xu, T. Okino, and K. Yamanouchi, J. Chem. Phys. **131**, 151101 (2009).

[44] X. Xie et al., Phys. Rev. Lett. **109**, 243001 (2012).

[45] E. Wells et al., Nat. Commun. **4**, 2895 (2013).

[46] T. Osipov, C. L. Cocke, M. H. Prior, A. Landers, Th. Weber, O. Jagutzki, L. Schmidt, H. Schmidt-Böcking, and R. Dörner, Phys. Rev. Lett. **90**, 233002 (2003).

[47] N. Saito, M. Nagoshi, M. Machida, I. Koyano, A. De Fanis, and K. Ueda, Chem. Phys. Lett. **393**, 295 (2004).

[48] J. I. Adachi, K. Hosaka, T. Teramoto, M. Yamazaki, N. Watanabe, M. Takahashi, and A. Yagishita, J. Phys. B **40**, F285 (2007).

[49] T. Osipov et al., J. Phys. B **41**, 091001 (2008).

[50] D. Duflot, J. M. Robbe, and J. P. Flament, J. Chem. Phys. **102**, 355 (1995).

[51] N. Chang, M. Shen, and C. Yu, J. Chem. Phys. **106**, 3237 (1997).

[52] T. S. Zyubina, Y. A. Dyakov, S. H. Lin, A. D. Bandrauk, and A. M. Mebel, J. Chem. Phys. **123**, 134320 (2005).

[53] M. E. A. Madjte, O. Vendrell, and R. Santra, Phys. Rev. Lett. **107**, 263002 (2011).

[54] A. N. Markevitch, D. A. Romanov, S. M. Smith, and R. J. Levis, Phys. Rev. Lett. **92**, 063001 (2004).

[55] V. S. Petrovic, J. Chem. Phys. **139**, 184309 (2013).